I&EC research
Industrial & Engineering Chemistry Research

Article

Cite This: Ind. Eng. Chem. Res. 2019, 58, 17885−17897

pubs.acs.org/IECR

Hybrid Model-Based Feedforward and Fractional-Order Feedback Control Design for the Benchmark Refrigeration System

Jie Yuan,*[,†] Zhenlong Wu,[‡] Shumin Fei,[†] and YangQuan Chen*[,§]

[†]Key Laboratory of Measurement and Control of CSE, Ministry of Education, School of Automation, Southeast University, Nanjing 210096, China

[‡]State Key Lab of Power System, Department of Energy and Power Engineering, Tsinghua University, Beijing 100084, China

[§]Mechatronics, Embedded Systems and Automation Lab, University of California, Merced, California 95343, United States

ABSTRACT: Refrigeration systems occupy a large proportion of the home energy consumption in the United States. Precise temperature management is a key point to enhance the energy utilization efficiency. Since proportional-integral-derivative (PID) controllers absolutely dominate control engineering, a large number of different control structures and theories have been developed to enhance the efficiency of PID controllers. A benchmark refrigeration system was proposed in PID2018 as a simulation platform for researchers to implement different control strategies. In this paper, a novel control strategy is designed for the benchmark refrigeration system, where the fractional-order lead-lag compensator is in consort with the baseline controllers and contributes to accelerate the system response by increasing the system bandwidth, and the feedforward compensators are utilized to compensate the disturbances in the benchmark problem. The simulation results given in the benchmark problem show the straightforward effectiveness of the proposed control structure compared to the existing control methods.

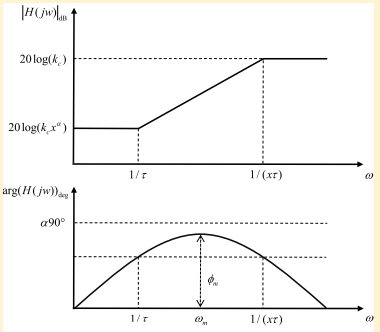

Asymptotic Bode plot of $H(s)$.

1. INTRODUCTION

It is reported that approximately 30% of total energy in the world is used for heating, ventilating, and air-conditioning, as well as by refrigerators and water heaters.[1] In the United States, refrigerators occupy approximately 28% of home energy consumption.[2] As a cutting-edge technology in the field of cooling generation, refrigeration consumes significant amount of energy during heating and cooling processes. The power consumption of each vapor-compression-based refrigeration system generally ranges from 1 kW to 1 MW. To enhance the energy utilization efficiency, the key issue is how to realize precise temperature management. The refrigeration system is a common and classic industrial application whose components are connected through various pipes and valves and the resulting strong nonlinearities and high coupling. The series of components in the refrigeration system work synergistically to hold temperature at the set-point. The disturbances wherever external or internal will deteriorate the control system, and it will damage the whole system if a fatal flaw exists in the control strategy.

Proportional-integral-derivative (PID) control has been widely accepted and used in industry especially for accuracy and optimized automatic control system, such as chemical processes,[3,4] refrigeration system,[5] hydrothermal power systems,[6] and autonomous vehicles.[7] It can be designed and tuned in a variety of operating conditions, unlike many other controllers that are much more complex but with marginal improvement. A number of PID tuning rules have been developed with practicability, such as the Ziegler−Nichols method,[8] frequency domain specifications,[9] SIMC tuning rules,[10] antiwindup adaptive PID control methods,[11] fuzzy control,[12] etc. However, the default tunings sometimes produce unsatisfactory performance under different conditions. With the recent development of intelligent control technology, PID controllers give new luster when combined with intelligent optimization algorithm,[13] PID neural network,[14] reinforcement learning technique,[15] etc. As PID control technique has a developing prospect in the future,[16] the proposed PID benchmark problem is essential and impendent to promote its development.[17] In this PID benchmark problem, initial PID controllers are given as a competitive baseline, and the control structure can be modified by researchers to improve the system performance.

It is widely known that feedforward control plays a significant role in disturbance rejection. There are a large amount of applications in the practical industry, such as disk drives,[18] pharmaceutical coating process,[19] and high-precision motion control.[20] The industry feedforward control technology has been reviewed.[21] In control systems, unknown disturbances can be compensated effectively by active disturbance rejection control method.[22,23] Additionally, some disturbances are measurable or preknown, which can be utilized to provide the major portion of the controller output. The control signal

Received: April 8, 2019
Revised: August 24, 2019
Accepted: August 31, 2019
Published: September 1, 2019

DOI: 10.1021/acs.iecr.9b01854
Ind. Eng. Chem. Res. 2019, 58, 17885−17897

of the feedforward control is not based on the tracking error, but on the mathematical model of the process and the measurement of the disturbance. In this case, oscillation can be effectively avoided, which improves the system performance without reducing stability. Although the plant model and the disturbance model are assumed to be exactly accurate, it is not always possible to remove the disturbance completely. It is clear that a feedforward controller always presents the inverse of the plant model. Conversing the control elements is not acceptable and achievable, when the plant model has nonminimum phase zeros or its delay is longer than that of the disturbance path model. As a result, it will lead to the instability or noncausality of the PID controller. To improve disturbance rejection, one alternative method is that the proper feedforward controller can be designed using optimal control strategy.[24] While the plant model cannot be conversed ideally, the disturbance will not be completely eliminated and the feedback may have a negative influence on the disturbance rejection. To remove the feedback influence from the feedforward design, the authors proposed a new feedforward control scheme that the disturbance has no effect on the feedback controller; thus, the feedforward controller and feedback controller can be designed separately.[25] Under this scheme, tuning rules for feedforward controller have been generalized under the case where the delay inversion is not realizable. The authors presented a performance index to evaluate the advantage of the feedforward controller compared to the structure in which PID controller is only implemented.[26] A good disturbance rejection by the feedforward controller relies on the accuracy of the process model and signal measurement. For the system with parameter uncertainties, a robust feedforward controller for a single-input-single-output (SISO) system is designed under the robust stability criterion.[27] The authors proposed a self-tuning feedforward controller for a multiple-input-multiple-output (MIMO) system to minimize loss of performance due to model uncertainties.[28] A robust feedforward controller originating from the internal model control idea for uncertain system is proposed by Vilanova et al., which generate a residual signal that determines the goodness of the models used for design.[29] A feedforward controller is adapted on-line using the filtered-x LMS (least mean squares) algorithm for disk drive systems, where the variations of system parameters between units are very common.[30] When the disturbance signal has measurement uncertainties due to the sensor calibration, sensor bandwidth limitation, noise, etc., a two-degree-of-freedom (DOF) controller is optimized under both model uncertainty and disturbance signal measurement uncertainty, and H_∞ tools are utilized to balance trade-off between performance and sensitivity to uncertainty.[31]

In classical control theory, the output feedback cannot assign the poles arbitrarily for which the dynamic specifications and static indicators cannot be achieved. A lead-lag compensator has the ability to avoid undesirable responses in a control system. As an important building block in the classical control theory, it is often utilized by engineers to achieve desired system zeros and poles or to reshape the open-loop system frequency response curve.[32] A phase-lead compensator increases the system stability and speed of the system response by increasing the system phase margin and bandwidth. In addition, a phase-lag compensator reduces the response steady-state error. The combination of the lead compensator and the lag compensator produces the synergistic effects which can improve the system performance in terms of stability, transient process, and steady-state error. As a generalization of the traditional compensator, the fractional-order lead-lag compensator contributes to a more flexible tuning ability with an additional parameter. One form of the fractional-order compensator is made up of the classical lead-lag compensator to the power of α.[33] In this paper, it is indicated that the this kind of fractional-order lead-lag compensator has larger lead region (the specified design point with respect to gain crossover frequency and phase margin in complex plane) than the traditional one. Khiabani and Babazadeh proposed an easier form which contains the fractional-order s^α, and this kind of fractional-order compensator can be easily implemented by the existing approximation techniques.[34] Yu and Wang proposed a performance assessment of the static lead-lag compensators for disturbance rejection in PID controlled systems.[35]

Herein, a developed control strategy is proposed to optimize temperature management for the benchmark refrigeration system. Based on the number of simulations, it is found that the fractional-order lead-lag compensator can significantly improve the system bandwidth, and subsequently accelerates the response speed. Meanwhile, the feedforward control we employed shows its strong function to compensate disturbances caused by external or internal variables.

Early partial results of this work have been reported where the employed control strategy has exhibited the ability to precisely control the system temperature.[36] This newly developed work obtains the enhanced performance with minimal modeling efforts. The main contributions of this paper are: (1) implementing all control strategies on a public benchmark refrigeration system that all results can be repeated and verified; (2) providing a logical and methodical procedure to analyze the fundamental characteristics of an MIMO system, such as nonlinearity and coupling degree; and (3) applying the fractional-order lead-lag compensator to improve the control performance, which has one more design freedom and outperforms the integer-order lead-lag compensator.

The remainder of this paper is organized as follows: Section 2 describes the controlled plant in the view of the control aspect. In Section 3, the refrigeration system is first analyzed in aspects of coupling and nonlinearity, and nominal models are also identified. The fractional-order lead-lag compensator is introduced in Section 4. The detailed design procedures of the feedforward controller are presented in Section 5. The simulation results shown in Section 6 demonstrate the effectiveness of the proposed structure. Finally, the paper is concluded in Section 7.

2. REFRIGERATION SYSTEM DESCRIPTION

The canonical one-compression-stage, one-load-demand refrigeration cycle is shown in Figure 1. The major objective of this cycle is to remove heat at the evaporator from its secondary flux and release heat at the condenser by exchanging it to the condenser secondary flux. Detailed operating principle of the refrigeration system can be found in ref 17, and the benchmark simulink files can be downloaded at http://servidor.dia.uned.es/~fmorilla/benchmarkPID2018/. The system variables are given in Table 1.

The output variable $T_{e,sec,out}$ is the outlet temperature of the evaporator secondary flux. In principle, the highest evaporator efficiency will be achieved when the refrigerant at the evaporator outlet is saturated vapor. However, this behavior

DOI: 10.1021/acs.iecr.9b01854
Ind. Eng. Chem. Res. 2019, 58, 17885−17897

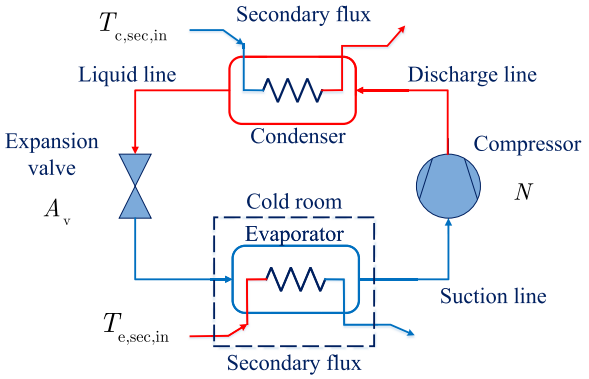

Figure 1. Schematic picture of one-compression-stage, one-load-demand vapor-compression refrigeration cycle (adapted from Figure 1 in ref 17).

Table 1. Refrigeration System Variables

variables		range
manipulated variables	A_v	10−100%
	N	30−50 Hz
output variables	$T_{sec,evap,out}$	
	T_{SH}	

is not acceptable in practice since the temperature of the evaporator outlet is very high in transient. The risk of liquid droplets formed when the evaporator outlet matches the compressor intake should be preferentially avoided. Thus, the degree of superheating, T_{SH}, serves as the second controlled signal. There are two manipulated variables in the benchmark problem such that A_v is the expansion valve opening position and N is the compressor speed, as shown in Figure 1. Seven variables stated in the PID2018 Benchmark documentation can be treated as disturbances.[17] The expansion valve, the compressor, and the thermal behavior of secondary fluxes are statically modeled since their dynamics are usually much faster than those of the evaporator and condenser. The major disturbances are the inlet temperature of the evaporator secondary flux $T_{e,sec,in}$ and the inlet temperature of the condenser secondary flux $T_{c,sec,in}$. Both of them should be compensated to achieve the better control in the benchmark problem. The initial operating point of the manipulated variables, output variables, and these two major disturbances are indicated in Table 2. Detailed information of the refrigeration system can be reviewed in ref 17.

3. PROBLEM FORMULATION

3.1. Coupling. In a controlled system, the coupling is the interaction between the controlled variables and manipulated variables. Depending on the coupling degree, the decoupling technology is then considered to be nor not to be applied to eliminate the interaction. It is thus crucial to first determine whether the coupling relationship exists in this two-inputs-two-outputs (TITO) refrigeration system. With this goal, we define the first input in the middle of the working range, as A_v = 55%, and the second one at initial value, N = 36.45 Hz. The system outputs are shown in Figure 2. Similarly, with N = 40 Hz and A_v = 48.79%, the corresponding outputs are shown in Figure 3. It is obvious that both two outputs have dependence on inputs, confirming that the refrigeration system is a coupled TITO system.

Table 2. Initial Operating Point

variables		range
manipulated variables	A_v	≅48.79%
	N	≅36.45 Hz (2187 rpm)
output variables	$T_{e,sec,out}$	≅−22.15 °C
	T_{SH}	≅14.65 °C
disturbances	$T_{c,sec,in}$	30 °C
	$T_{e,sec,in}$	−20 °C

Subsequently, a nominal model should be built to analyze the coupling degree and to determine whether the decoupling strategy should be implemented. Although several modeling works for the similar system have already been done in published reports,[37−40] these proposed models seem to be complicated technically. Since the system is a black box in SIMULINK form, there exists an increased difficulty in establishing an accurate model for who has little knowledge about the TITO system. To simplify the modeling work, we employ the step change of input variables to identify the system in form of transfer functions. The calculation is carried out in SIMULINK environment. The nominal system is defined as the case where the manipulated variables are working at the middle point of their working range.

The detailed modeling procedures for the refrigeration system are given as follows:

1. Remove all of the control elements, such as the controllers and feedbacks.
2. Keep N = 36.45 Hz, working at initial value.
3. Set 48.79 as the initial value of the manipulated variable A_v and add a step change to 55 at 200 (s). One can get the system response, as shown in Figure 2.
4. Identify the transfer functions from A_v to $T_{e,sec,out}$ and from A_v to T_{SH}.
5. Keep A_v = 48.79%.
6. Set 36.45 as the initial value of the manipulated variable N and add a step change to 40 at 200 (s). One can get the system response, as shown in Figure 3.
7. Identify the transfer functions of the step transient from N to $T_{e,sec,out}$ and T_{SH}.

The nominal model of the TITO system is identified as

$$G_{11}(s) = \frac{T_{e,sec,out}(s)}{A_v(s)} = \frac{-0.6016s - 0.01141}{s^2 + 15.97s + 0.5954} \quad (1)$$

$$G_{21}(s) = \frac{T_{SH}(s)}{A_v(s)} = \frac{-4.616s - 0.1283}{s^2 + 11.37s + 0.427} \quad (2)$$

$$G_{12}(s) = \frac{T_{e,sec,out}(s)}{N(s)} = \frac{-0.002224s - 0.0002071}{s^2 + 3.27s + 0.1062} \quad (3)$$

$$G_{22}(s) = \frac{T_{SH}(s)}{N(s)} = \frac{3.126s + 0.06653}{s^2 + 16.3s + 0.3764} \quad (4)$$

Once these four transfer functions are obtained, the square complex matrix G is represented according to

$$G(s) = \begin{bmatrix} G_{11}(s) & G_{12}(s) \\ G_{21}(s) & G_{22}(s) \end{bmatrix} \quad (5)$$

and the relative gain array (RGA) of matrix 5 is given as[41]

DOI: 10.1021/acs.iecr.9b01854
Ind. Eng. Chem. Res. 2019, 58, 17885−17897

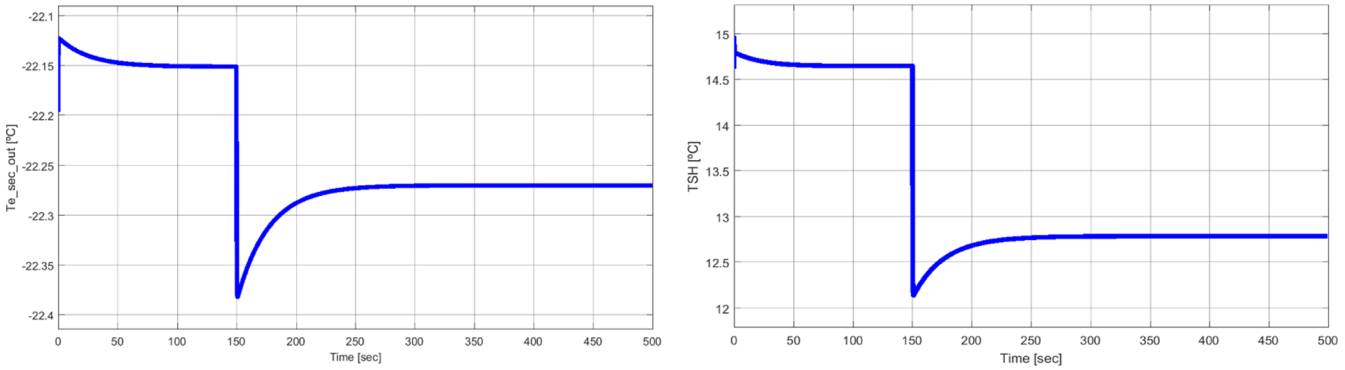

Figure 2. System outputs under single input A_v = 55%.

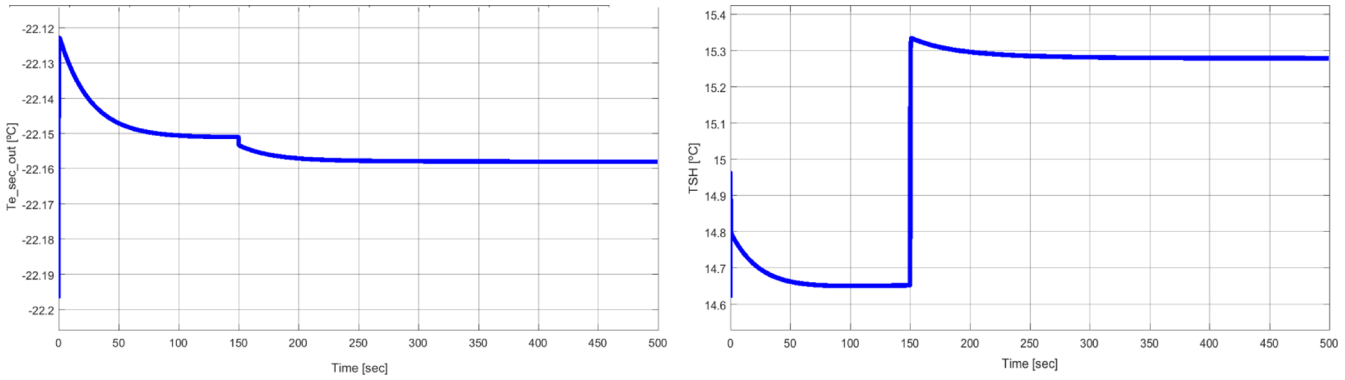

Figure 3. System outputs under single input N = 40 Hz.

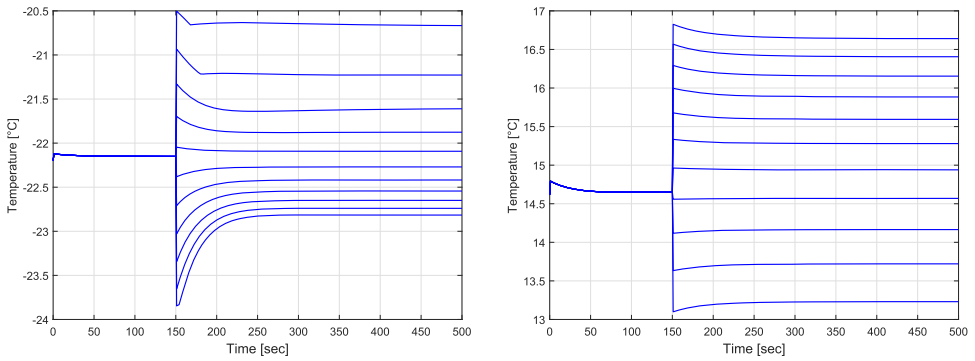

(a) A_v - $T_{e,sec,out}$ (b) N - T_{SH}

Figure 4. System responses under different step inputs.

$$\mathrm{RGA}(G) = \Lambda(G) \triangleq G(0) \times (G^{-1}(0))^{\mathrm{T}} = \begin{bmatrix} 0.8525 & 0.1475 \\ 0.1475 & 0.8525 \end{bmatrix} \tag{6}$$

The value in the leading diagonal, 0.8525, is close to unity, which means the coupling inside the system is not very serious and can be ignored. In this situation, our discussion can be simplified greatly. The control pairing can be chosen such that A_v controls $T_{e,sec,out}$ and N controls T_{SH}. Therefore, the TITO refrigeration system is considered approximately as two SISO systems.

3.2. Nonlinearity. In the refrigeration control system, components are connected through various pipes and valves in a closed cycle, which may form strong nonlinearities. To provide good control performance, the nominal model needs to be supplemented to compensate the nonlinear behaviors. A simple procedure is therefore designed to have a intuitive observation of the nonlinearity in these two SISO systems. We keep one input at its initial value and scan other input with a constant sample interval (11 points per input range). The system responses with various step inputs are shown in Figure 4.

The two channels show nonlinearity not only in transient processes but also in steady-state gain under different manipulated input values. To analyze the nonlinearity degree of the refrigeration system, the gap metric is applied to this TITO system. The gap metric provides a measurement of the distance between two linear time invariant systems (LTIs).[42,43] It is widely used in nonlinear chemical control systems.[44−46] The gap between two linear systems is defined as

$$\delta(G_1, G_2) = \max\{\vec{\delta}(G_1, G_2), \vec{\delta}(G_2, G_1)\} \tag{7}$$

DOI: 10.1021/acs.iecr.9b01854
Ind. Eng. Chem. Res. 2019, 58, 17885−17897

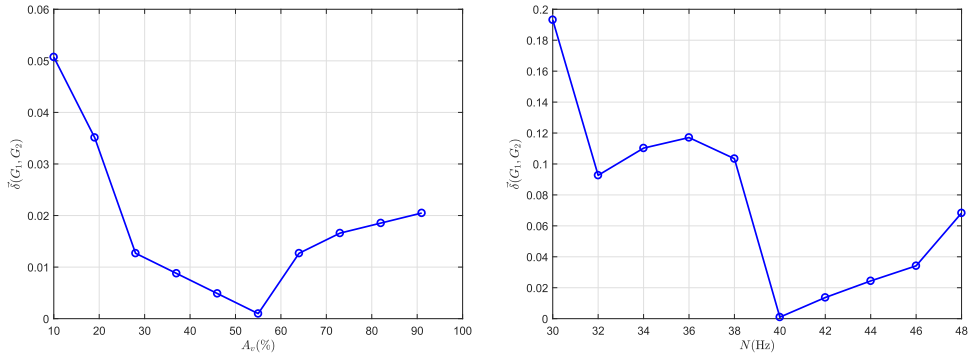

(a) A_v - $T_{e,sec,out}$ (b) N - T_{SH}

Figure 5. Gap measurement of different operating points within SISO systems.

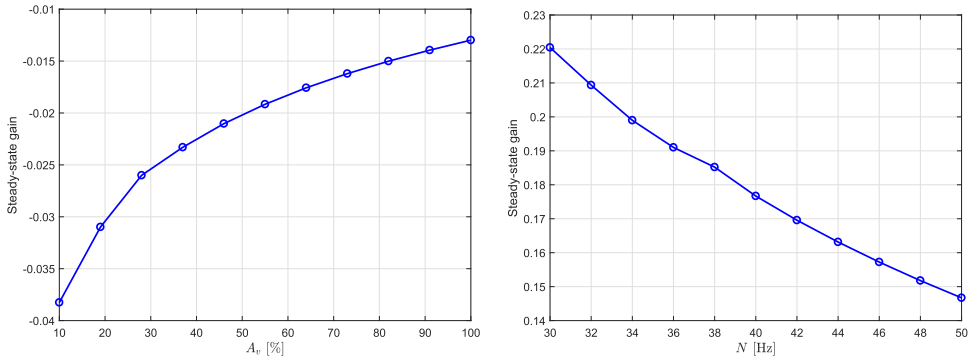

(a) A_v - $T_{e,sec,out}$ (b) N - T_{SH}

Figure 6. System steady-state gain under different step inputs.

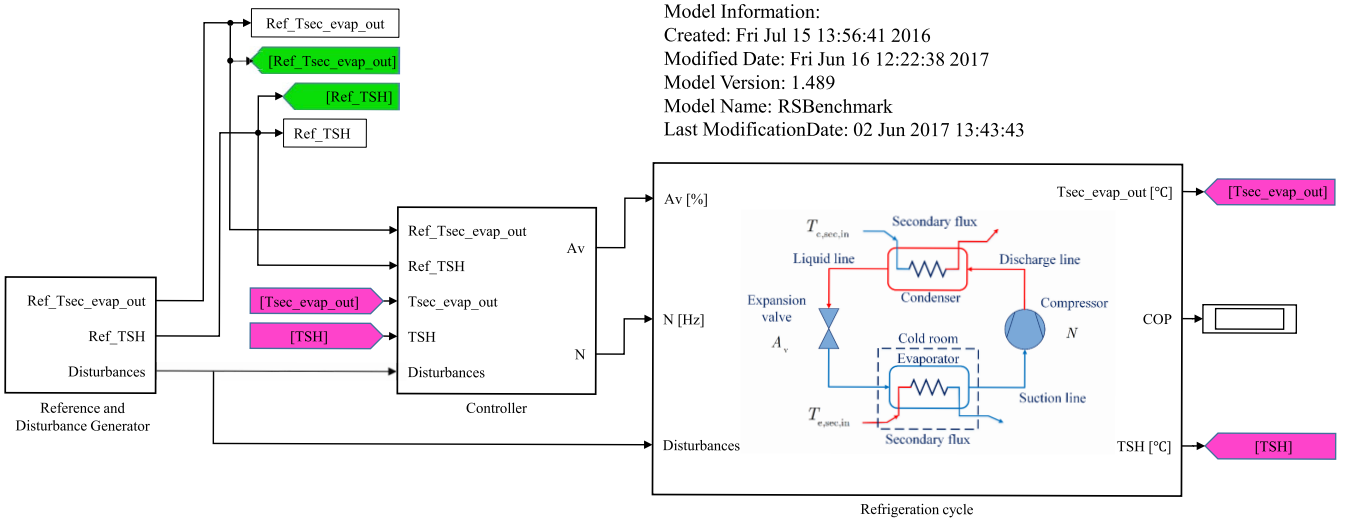

Figure 7. Refrigeration control system.

where G_1 and G_2 are the system transfer functions which are linearized around the nominal and an arbitrary operating points, respectively, and $\vec{\delta}(G_1,G_2)$ is the directed gap, which is defined as

$$\vec{\delta}(G_1, G_2) = \inf_{Q \in H_\infty} \left\| \begin{bmatrix} M_1 \\ N_1 \end{bmatrix} - \begin{bmatrix} M_2 \\ N_2 \end{bmatrix} Q \right\|_\infty \tag{8}$$

where $G_1 = N_1 M_1^{-1}$ and $G_2 = N_2 M_2^{-1}$ are normalized co-prime factorizations of two linear systems, and Q is a matrix parameter which has finite H_∞ norm. For any two linear systems, the gap is restricted with

$$0 \le \vec{\delta}(G_1, G_2) \le 1 \tag{9}$$

Let G_1 represents the nominal operating point of the refrigeration system, A_v = 55% and N = 40 Hz. By testing the above 11 operating points, the gap between these two SISO systems is plotted in Figure 5. The gap distance between non-nominal operating points and nominal operating point in the first control loop is small, thus the nonlinearity is small.

DOI: 10.1021/acs.iecr.9b01854
Ind. Eng. Chem. Res. 2019, 58, 17885−17897

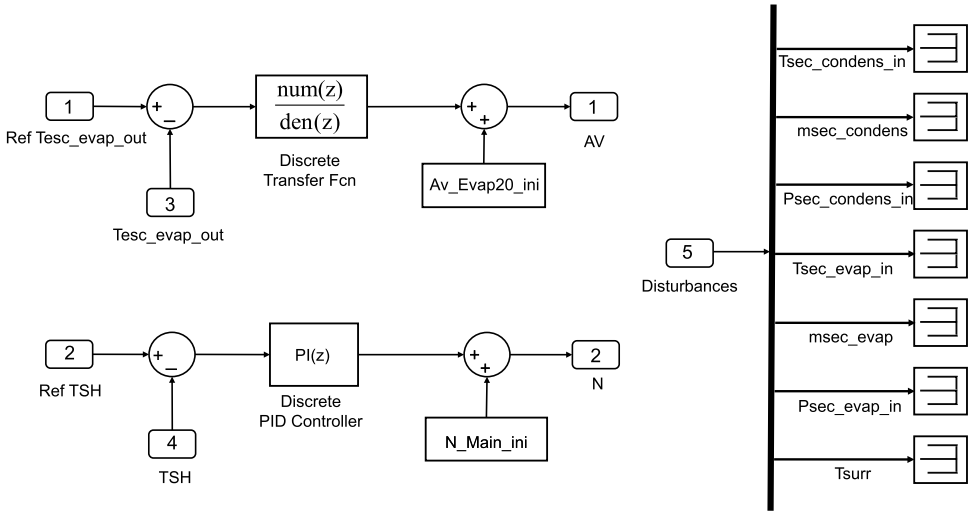

Figure 8. Discrete decentralized controller included by default in the refrigeration control system.

The second control loop shows greater nonlinearity under different operating points.

For the minimal modeling efforts and nonlinearity compensation efforts, only the steady-state gains for two SISO systems are compensated. The calculated steady-state gain are shown in Figure 6. Two lookup tables are generated based on the steady-state gains to minimize the nonlinear effect. These two lookup tables are injected after the control signals in the feedforward loops to mitigate the effects of nonlinearities.

3.3. Control Structure. Referring to the Benchmark PID2018 instructive document,[17] the closed-loop refrigeration system and the default multivariable controller structure are shown in Figures 7 and 8, respectively. The transfer functions of discrete decentralized controllers, with sampling period 1 (s), are given as

$$C_1(z^{-1}) = C_{T_{e,sec,out}-A_v}(z^{-1}) = \frac{-1.0136 - 0.0626z^{-1} + 0.9988z^{-2}}{1 - 1.9853z^{-1} + 0.9853z^{-2}} \quad (10)$$

$$C_2(z^{-1}) = C_{T_{SH}-N}(z^{-1}) = \frac{0.42 - 0.02z^{-1}}{1 - z^{-1}} \quad (11)$$

The controllers in continuous time domain are

$$C_1(s) = C_{T_{e,sec,out}-A_v}(s) = \frac{-1.014s^2 - 2.066s - 0.07797}{s^2 + 0.01481s - 4.505 \times 10^{-16}} \quad (12)$$

$$C_2(s) = C_{T_{SH}-N}(s) = 0.22 + \frac{0.4}{s} \quad (13)$$

Based on the aforementioned system analysis, the loop transfer functions of the controlled refrigeration system can be obtained

$$L_1(s) = C_1(s)G_{11}(s) = \frac{0.6098s^3 + 1.255s^2 + 0.07049s + 0.000889}{s^4 + 15.98s^3 + 0.8319s^2 + 0.008817s - 2.682 \times 10^{-16}} \quad (14)$$

$$L_2(s) = C_2(s)G_{22}(s) = \frac{1.313s^2 + 1.278s + 0.02661}{s^3 + 16.3s^2 + 0.3764s} \quad (15)$$

The closed-loop system responses under the default controller are shown in Figure 9.

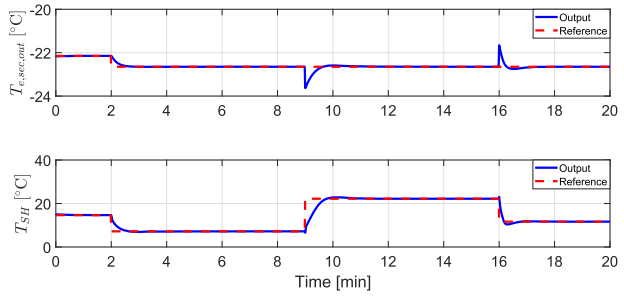

Figure 9. System responses under the default controller.

4. FREQUENCY DOMAIN SYNTHESIS OF THE FRACTIONAL-ORDER LEAD-LAG COMPENSATOR

It can be obviously seen in Figure 9 that the default controller generates stable but slow responses. It is known that a system with a higher gain crossover frequency has faster responses. Generally, a higher gain crossover frequency can be achieved by cascading a compensation element to the original open-loop system. The lead-lag compensator plays an important role in the control theory since it can improve the undesirable performance of the controlled system in the frequency domain. The fractional-order lead-lag compensator is a generalization of traditional one, which can obtain more satisfactory results using an additional tunable parameter.

A fractional-order lead-lag compensator is in the form

$$H(s) = k_c\left(\frac{s + 1/\tau}{s + 1/(x\tau)}\right)^{\alpha} = k_c x^{\alpha}\left(\frac{\tau s + 1}{x\tau s + 1}\right)^{\alpha} \quad (16)$$

where $x > 0$ and $0 < \alpha < 2$. The asymptotic approximation example of the Bode plot of fractional-order phase-lead compensator is shown in Figure 10. After simple deduction, the following frequency domain characteristics can be established

DOI: 10.1021/acs.iecr.9b01854
Ind. Eng. Chem. Res. 2019, 58, 17885−17897

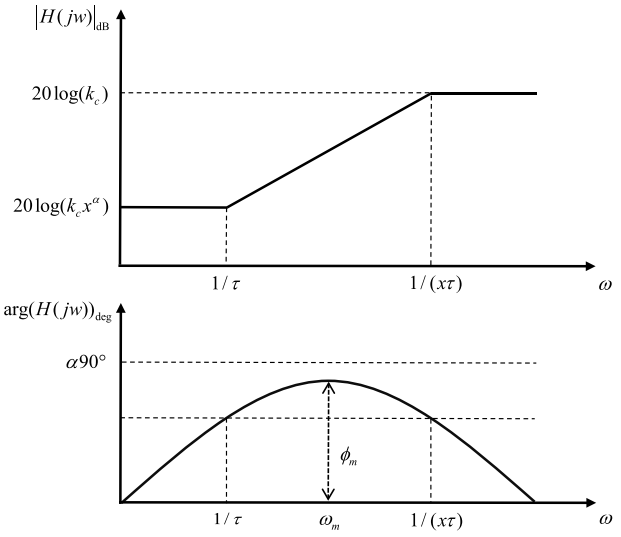

Figure 10. Asymptotic Bode plot of $H(s)$.

$$w_{\mathrm{m}} = \frac{1}{\tau\sqrt{x}} \tag{17}$$

$$\phi_{\mathrm{m}} = \alpha \arcsin\left(\frac{1-x}{1+x}\right) \tag{18}$$

$$\left|\frac{H(\mathrm{j}w_{\mathrm{m}})}{k_{\mathrm{c}}x^{\alpha}}\right| = \left|\frac{1+\mathrm{j}\tau w_{\mathrm{m}}}{1+\mathrm{j}x\tau w_{\mathrm{m}}}\right|^{\alpha} = \left(\frac{1}{\sqrt{x}}\right)^{\alpha} \tag{19}$$

Phase-lead compensators and phase-lag compensators are two general types of compensators. Either one with magnitude over 0 dB can devote to increasing system gain crossover frequency w_{c} and accordingly, increasing the system bandwidth. It should be noted that the increasing w_{c} will decrease the phase margin of the original system. Nevertheless, the phase-lead compensator raises the phase bode plot up, which leads to a higher phase margin. Given these facts, the phase-lead compensator increases the gain crossover frequency w_{c} of the open-loop system, but cannot guarantee a higher phase margin. Thus, when designing and implementing the phase-lead compensator, the desired specification w_{c}^{*} should be greater than the original value. The desired phase margin φ_{m}^{*} can be designed through trial and error. The parameters of the compensator can be determined according to the following equations

$$w_{\mathrm{m}} = \frac{1}{\tau x} = w_{\mathrm{c}}^{*} \tag{20}$$

$$\alpha\arcsin\left(\frac{1-x}{1+x}\right) = -\pi + \varphi_{\mathrm{m}}^{*} + \arg(L)|_{w=w_{\mathrm{c}}^{*}} \tag{21}$$

$$|k_{\mathrm{c}}(\sqrt{x})^{\alpha}| = \frac{1}{|L(\mathrm{j}w_{\mathrm{c}}^{*})|} \tag{22}$$

where L is the loop transfer function of the controlled system. By scanning the different values of α, for each fixed α, three other parameters can be uniquely obtained.

5. DISTURBANCE FEEDFORWARD COMPENSATOR DESIGN

In the SIMULINK operation of the refrigerator system, main disturbances are the inlet temperature of the evaporator secondary flux $T_{\mathrm{e,sec,in}}$ and the condenser secondary flux $T_{\mathrm{c,sec,in}}$. These two parameters have step changes as shown in Figure 11.

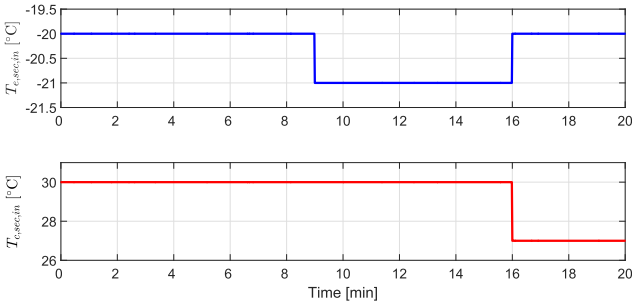

Figure 11. Standard simulation for PID2018 Benchmark generating changes in two disturbances: $T_{\mathrm{e,sec,in}}$ and $T_{\mathrm{c,sec,in}}$.

Feedforward compensation technique has been widely used in disturbance rejection. The disturbance feedforward control diagram for an SISO system is shown in Figure 12, where $C(s)$,

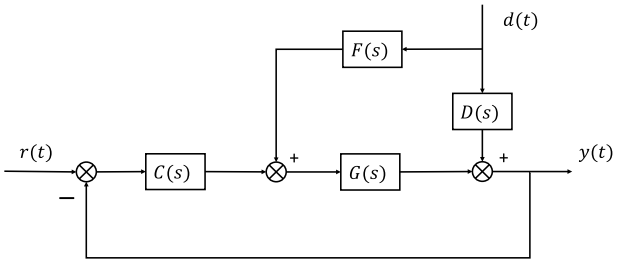

Figure 12. Feedforward control structure of disturbance rejection for an SISO system.

$G(s)$, $d(t)$, $D(s)$, $F(s)$, $r(t)$, and $y(t)$ represent the controller, plant, disturbance signal, disturbance path model, feedforward compensator, the system reference and output, respectively.

The feedforward controller is designed to eliminate the effect of the disturbance signal before they affect the system. On this basis, the following equation is obtained as

$$D_{\mathrm{t}}(s)F(s)G(s) + D_{\mathrm{t}}(s)D(s) = 0 \tag{23}$$

where $D_{\mathrm{t}}(s)$ is the Laplace transform of the disturbance signal $d(t)$. Thus, the feedforward compensator is derived as

$$F(s) = -\frac{D(s)}{G(s)} \tag{24}$$

Although feedforward control is a very mature technique in control theory, there are few references or tutorials that show the detailed procedures of designing a feedforward controller. In the following, the feedforward controller design procedures will be introduced in detail. The critical first step is to model the disturbance path $D(s)$. There are two disturbances in this Benchmark problem. As shown in Figure 11, $T_{\mathrm{e,sec,in}}$ has a step decrease at 9 (min) and a step increase at 16 (min), while $T_{\mathrm{c,sec,in}}$ has a step decrease at 16 (min). When modeling the disturbance path, only one disturbance should be implemented to the system, thus another disturbance should be compensated as a constant value at first. In addition, the disturbance path modeling should be done in the open-loop situation, which means that the controller cannot be served as a modeling element. Taking the disturbance rejection $T_{\mathrm{e,sec,in}}$ as

DOI: 10.1021/acs.iecr.9b01854
Ind. Eng. Chem. Res. 2019, 58, 17885−17897

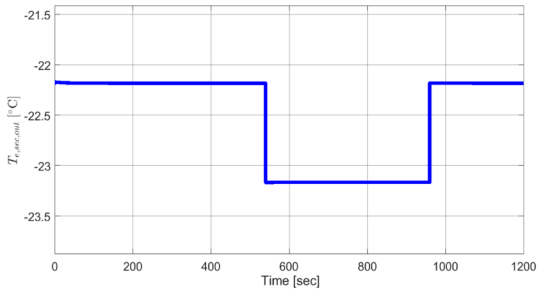

(a) The $T_{e,sec,out}$ response under the disturbance $T_{e,sec,in}$.

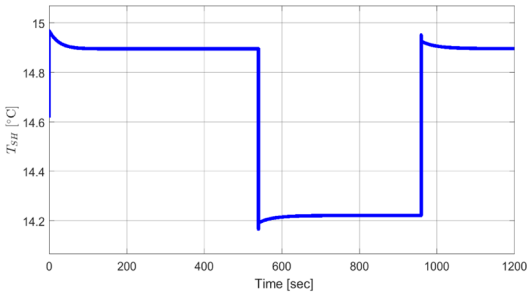

(b) The T_{SH} response under the disturbance $T_{e,sec,in}$.

Figure 13. System responses under the disturbance $T_{e,sec,in}$.

an example, the feedforward compensator design procedures are as follows

1. Cut off the two feedbacks in the closed-loop system and set the reference signals of $T_{e,sec,out}$ and T_{SH} as zero to make sure the controllers do not work.
2. Compensate the disturbance $T_{c,sec,in}$ as a constant value, which equals 30.
3. Implement the disturbance $T_{e,sec,in}$ into the system and get the responses shown in Figure 13.
4. Capture the transient processes of the output $T_{e,sec,out}$ and T_{SH} and identify the disturbance path models $D_{11}(s)$ and $D_{21}(s)$.
5. Generate two feedforward compensators according to eq 24.
6. Add the compensation signals to their corresponding controller signals.

The calculated procedure regarding disturbance rejection of $T_{c,sec,out}$ is repeated so that four disturbance path models are given as

$$D_{11}(s) = \frac{T_{e,sec,out}(s)}{T_{e,sec,in}(s)} = \frac{44.84}{s + 45.58} \tag{25}$$

$$D_{21}(s) = \frac{T_{SH}(s)}{T_{e,sec,in}(s)} = \frac{-109.1s + 4.903}{s^2 + 256.4s + 7.268} \tag{26}$$

$$D_{12}(s) = \frac{T_{e,sec,out}(s)}{T_{c,sec,in}(s)} = \frac{0.008624}{s + 0.04323} \tag{27}$$

$$D_{22}(s) = \frac{T_{SH}}{T_{c,sec,in}} = \frac{0.572}{s + 0.04099} \tag{28}$$

As a discrete-time control component, the feedforward controllers are implemented in discrete time. Hence, the compensators are regenerated as digital filters with sampling period 1 (s)

$$F_{11}(z) = \frac{28.35^2 - 5.283z - 21.22}{z^2 - 0.06528z - 0.8987} \tag{29}$$

$$F_{21}(z) = \frac{2.328z^3 - 2.958z^2 - 1.33z + 1.902}{z^3 - 0.9665z^2 - 0.9692z + 0.9368} \tag{30}$$

$$F_{12}(z) = \frac{0.127z^2 - 0.02366z - 0.09502}{z^2 - 1.939z + 0.9397} \tag{31}$$

$$F_{22}(z) = \frac{-0.164z^2 + 0.03214z + 0.1252}{z^2 - 1.939z + 0.9396} \tag{32}$$

Then, F_{11} and F_{12} can be added after the first controller to compensate the manipulated signal A_v. F_{21} and F_{22} can be added after the second controller to compensate the manipulated signal N. The total controller structure is illustrated in Figure 14.

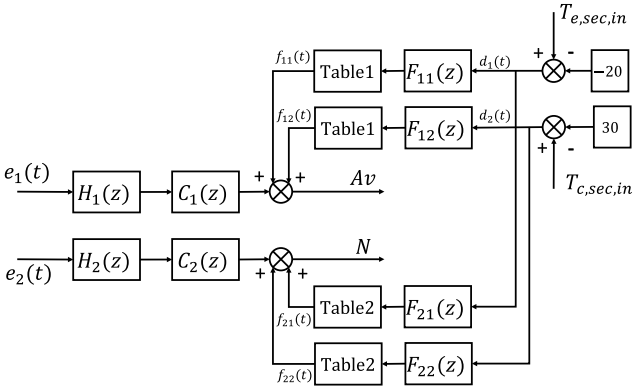

Figure 14. Overall control structure including the disturbance feedforward controllers and lead-lag compensators.

Remark 1. This paper is written for the benchmark refrigeration system which is proposed in the 2018 IFAC Conference on Advances in proportional-integral-derivative control. The results obtained in this paper can be easily and fairly compared to other papers published in this conference.

Remark 2. This paper proposed a practical design method to improve the system performance significantly while keeping the original controller type and parameters. Minimal modeling efforts are made to mitigate the nonlinearity of the Benchmark system. The disturbance feedforward compensation procedures are given in detail and can be easily followed and operated by someone who has the control background. The order α in the fractional-order lead-lag compensator is an additional parameter that provides higher potential to enhance the system performance.

6. SIMULATION RESULTS

Depending on the phase-lead-lag technique and the feedforward control strategy introduced previously, five controllers are defined for simplicity. Controller 1 ($C1$) is the default controller (eqs 12 and 13),[17] and controller 2 ($C2$) is the second competitive baseline provided in the Benchmark PID2018 documentation, which are not visible to readers.

DOI: 10.1021/acs.iecr.9b01854
Ind. Eng. Chem. Res. 2019, 58, 17885−17897

Controller 3 ($C3$) is made up of the default controller and the feedforward compensator. Controller 4 ($C4$) is the combination of the default controller, the feedforward compensator, and the lead-lag compensator. Before showing the simulation results, the individual assessment indices and the combined index provided in the instructive document are given as follows[17]

$$\mathrm{IAE}_i = \int_0^{\mathrm{time}} |e_i(t)|\, dt \tag{33}$$

$$\mathrm{ITAE}_i = \int_0^{t_c+t_s} (t - t_c)|e_i(t)|\, dt \tag{34}$$

$$\mathrm{IAVU}_i = \int_0^{\mathrm{time}} \left|\frac{du_i(t)}{dt}\right| dt \tag{35}$$

$$\mathrm{RIAE}_i(C_{\mathrm{new}}, C_{\mathrm{old}}) = \frac{\mathrm{IAE}_i(C_{\mathrm{new}})}{\mathrm{IAE}_i(C_{\mathrm{old}})} \tag{36}$$

$$\mathrm{RITAE}_i(C_{\mathrm{new}}, C_{\mathrm{old}}, t_c, t_s) = \frac{\mathrm{ITAE}_i(C_{\mathrm{new}}, t_c, t_s)}{\mathrm{ITAE}_i(C_{\mathrm{old}}, t_c, t_s)} \tag{37}$$

$$\mathrm{RIAVU}_i(C_{\mathrm{new}}, C_{\mathrm{old}}) = \frac{\mathrm{IAVU}_i(C_{\mathrm{new}})}{\mathrm{IAVU}_i(C_{\mathrm{old}})} \tag{38}$$

$$\begin{aligned} J(C_{\mathrm{new}}, C_{\mathrm{old}}) = [&w_1\mathrm{IAE}_1(C_{\mathrm{new}}, C_{\mathrm{old}}) + w_2\mathrm{RIAE}_2(C_{\mathrm{new}}, C_{\mathrm{old}}) \\ &+ w_3\mathrm{RITAE}_1(C_{\mathrm{new}}, C_{\mathrm{old}}, t_{c1}, t_{s1}) + w_4\mathrm{RITAE}_2(C_{\mathrm{new}}, C_{\mathrm{old}}, t_{c2}, t_{s2}) \\ &+ w_5\mathrm{RITAE}_2(C_{\mathrm{new}}, C_{\mathrm{old}}, t_{c3}, t_{s3}) + w_6\mathrm{RITAE}_2(C_{\mathrm{new}}, C_{\mathrm{old}}, t_{c4}, t_{s4}) \\ &+ w_7\mathrm{RIAVU}_1(C_{\mathrm{new}}, C_{\mathrm{old}}) + w_8\mathrm{RIAVU}_2(C_{\mathrm{new}}, C_{\mathrm{old}})]/\sum_1^8 w_i \end{aligned} \tag{39}$$

where C_{old} represents the competitive baseline controller and C_{new} represents the revised controller. The index in $[0, 1)$ indicates that C_{new} is better than C_{old}, and $(1, \infty)$ indicates that C_{new} is worse than C_{old}. The smaller the value is, the better performance of the second controller has. It should be noted that the realization of eqs 33−39 is written in ".p" files in MATLAB, which are inaccessible to readers. The values of the weight parameters w_i are unknown and the dominant performance index is inaccessible; thus, the readers cannot emphasize on a specific control strategy to improve the performance. Under these conditions, the competition of control strategies on the benchmark problem is challenged, fair, and impartial.

First, to assess the effectiveness of the disturbance feedforward compensation, new compensators based on eqs 29−32 are applied without the lead-lag compensation. The system time responses for $C3$ are shown in Figure 15. The compensation signals generated by the feedforward controllers are shown in Figure 16, and the manipulated signals are shown in Figure 17. It is worth noting that the feedforward compensation signal F_{22} with an amplitude higher than 20 (the working range of N) will make N get saturated immediately and last until the end. To avoid this case, we remove this signal from the control structure. From Figure 15, when disturbances occur at 9 (min) and 16 (min), the responses for feedforward compensated system departure the reference signal and then quickly return back to the set-point. This observation can be ascribed to the compensation signal that accelerates the disturbance rejection. It can be found from Figure 17 that the compensation signals greatly shorten the

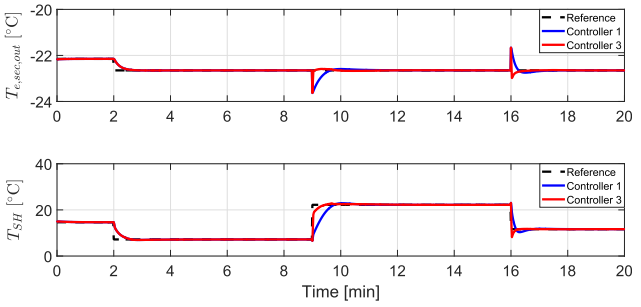

Figure 15. Qualitative comparison between $C3$ and $C1$ with the MIMO refrigeration control system; controlled variables.

saturated duration of A_v and N compared to the default controller.

Then, the fractional-order lead-lag compensators are designed to accelerate the system responses by increasing the system crossover frequency. The gain crossover frequency and phase margin for loop 14 are w_{c1} = 0.0779 rad/s and φ_{m1} = 88.4°, respectively. To achieve the relatively best results, by cascading a lead-lag compensator, the desired gain crossover frequency is selected with an equal interval 0.1 from the range [0.1,0.5] rad/s. The original phase margin is large enough to ensure the robustness of the closed-loop system. Considering the system response will become slow under the large phase margin condition, the desired phase margin is selected from the range [58°, 110°] with an equal interval 4°. For the loop 15 where w_{c2} = 0.0766 rad/s and φ_{m2} = 95.6°, the desired crossover frequency range is the same with loop 14, and the desired phase margin is selected from the range [41°, 105°] with an equal interval 4°. While designing the lead-lag compensators, the fractional-order α is chosen from [0.1,1.9] with an equal interval 0.1 rad/s. With each fixed α and the specifications, the compensators can be obtained by solving eqs 20−22. It should be noted that some of the specification combination will have no solution when solving these three equations.

With the combination of feedforward controllers, the lead-lag compensator for the loop 14 is first applied. The cost values with respect to three variables are plotted in Figure 18. The cost values are represented by the color, and the blank points in the figure means that there is no solution under the corresponding specifications. The optimal design specifications and the least cost value are given in Table 3. The corresponding lead-lag compensator is

$$H_1(s) = 6.8406\left(\frac{2.3303s + 1}{1.7165s + 1}\right)^{0.5} \tag{40}$$

With the implementation of $H_1(s)$, the lead-lag compensator for loop 15 is cascaded and the cost values under different design specifications are plotted in Figure 19. Optimal design specifications are given in Table 3, and the corresponding compensator is

$$H_2(s) = 1.5456\left(\frac{1.4975s + 1}{7.4199s + 1}\right)^{1.1} \tag{41}$$

The implementation of eqs 40 and 41 is realized with integer fifth-order transfer functions

$$\hat{H}_1(s) = \frac{6.851s^5 + 35.6s^4 + 71.59s^3 + 72.7s^2 + 40.42s + 8.359}{s^5 + 5.271s^4 + 10.83s^3 + 11.25s^2 + 6.431s + 1.423} \tag{42}$$

DOI: 10.1021/acs.iecr.9b01854
Ind. Eng. Chem. Res. 2019, 58, 17885−17897

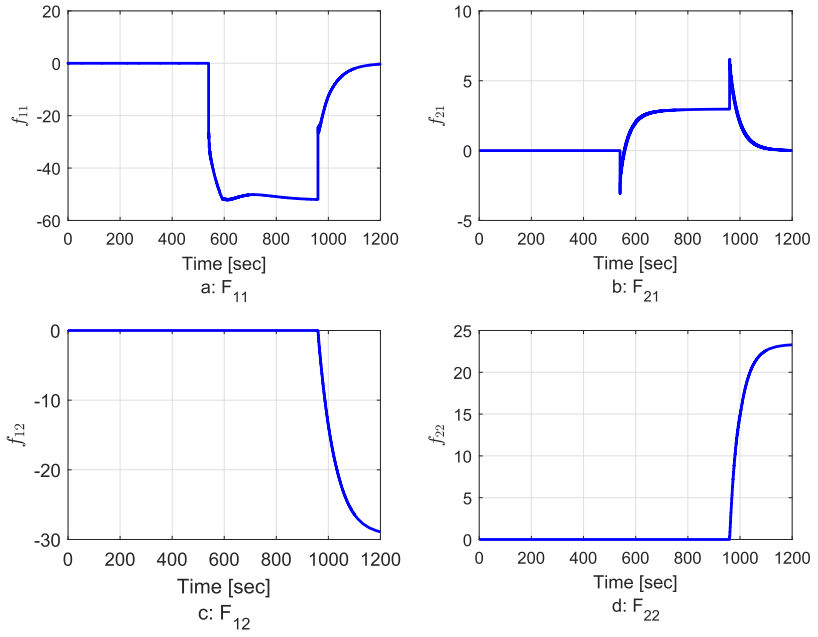

Figure 16. Feedforward compensation signals.

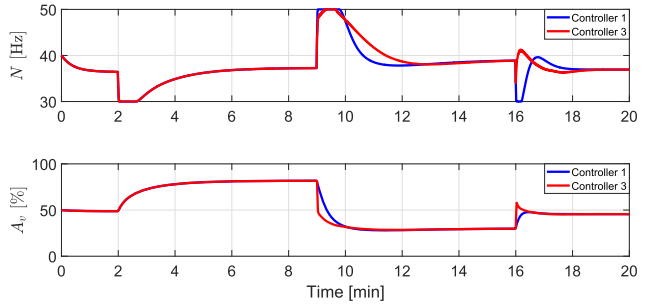

Figure 17. Qualitative comparison between $C3$ and $C1$ with the MIMO refrigeration control system; manipulated variables.

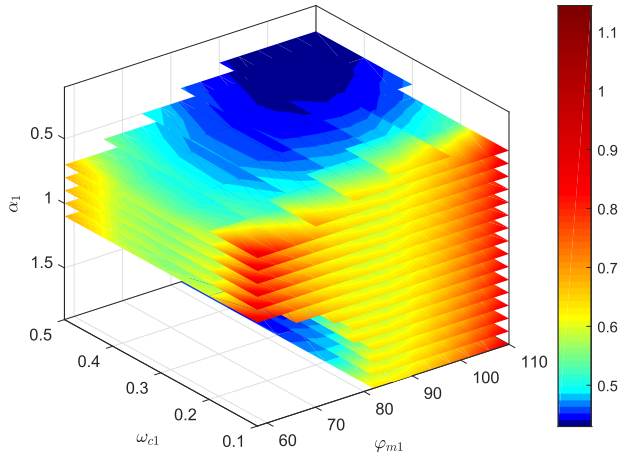

Figure 18. Cost value J when the system is equipped with the disturbance feedforward compensators and the fractional-order lead-lag compensator in loop 14.

$$\hat{H}_2(s) = \frac{1.544s^5 + 5.94s^4 + 14.21s^3 + 15.19s^2 + 9.512s + 3.105}{s^5 + 3.254s^4 + 7.379s^3 + 5.669s^2 + 3.337s + 0.3444} \tag{43}$$

The approximations of the fractional-order compensators can be implemented via the MATLAB command `fitmagfrd(.)`

Table 3. Optimal Design Specifications of the Loops Compensated by Fractional-Order Lead-Lag Controllers

loop	$\omega^*_{c1,2}$	$\varphi^*_{m1,2}$	$\alpha_{1,2}$	J
$T_{e,sec,out} - A_v$	0.5	106	0.5	0.4299
$T_{SH} - N$	0.3	61	1.1	0.2838

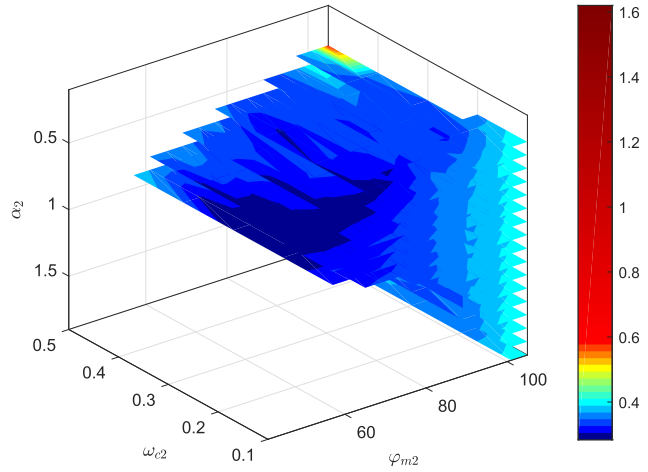

Figure 19. Cost value J when the system is equipped with the disturbance feedforward compensators and the fractional-order lead-lag compensator in loops 14 and 15.

in "Robust Control Toolbox". Bode plots of these two compensators and corresponding implementations are given in Figures 20a and 21a. Bode plots of the original loop transfer function and the compensated open-loop transfer function are shown in Figures 20b and 21b. It is seen that $H_1(s)$ is a fractional-order phase-lead compensator and $H_2(s)$ is a fractional-order phase-lag compensator. Both of the compensators form positive magnitude, demonstrating the increase of the gain crossover frequency, which results in faster system responses. Comparisons of simulated system responses and control signals between $C1$ and $C4$ are shown in Figures 22 and 23, respectively. In the time interval 2−9 min, no

DOI: 10.1021/acs.iecr.9b01854
Ind. Eng. Chem. Res. 2019, 58, 17885−17897

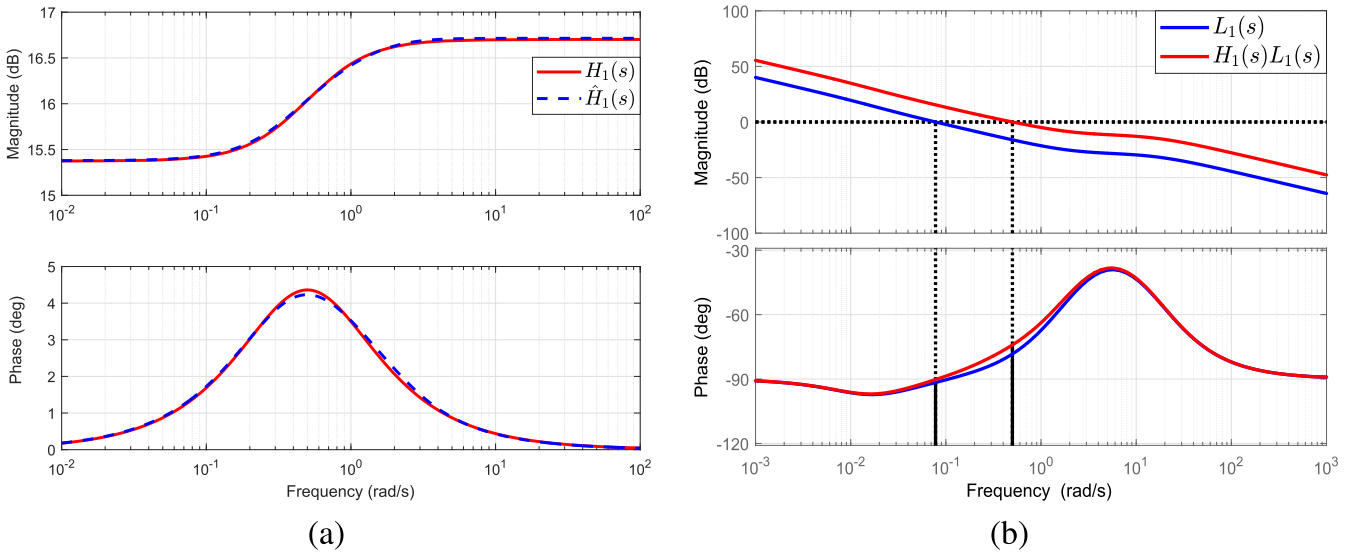

Figure 20. Bode plots of $H_1(s)$ and implementation of $\hat{H}_1(s)$ (a). Bode plots of uncompensated and compensated open-loop system for the loop A_v – $T_{e,sec,out}$ (b).

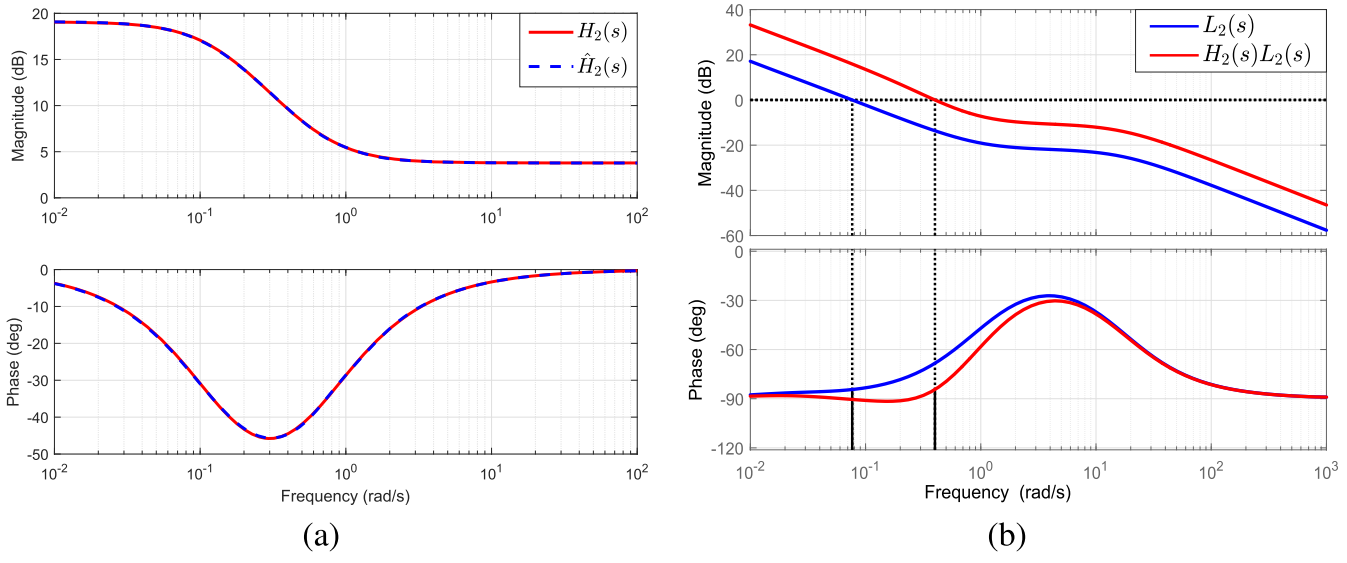

Figure 21. Bode plots of $H_2(s)$ and implementation of $\hat{H}_2(s)$ (a). Bode plots of uncompensated and compensated open-loop system for the loop N – T_{SH} (b).

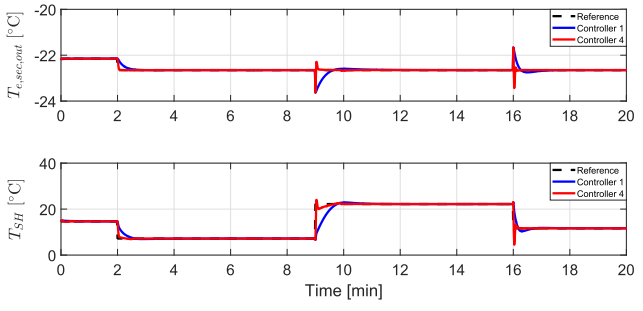

Figure 22. Qualitative comparison between C4 and C1 with the MIMO refrigeration control system; controlled variables.

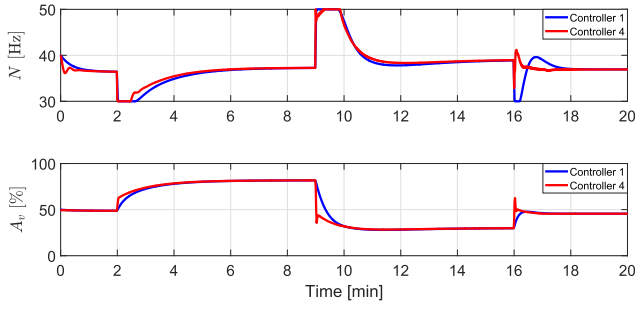

Figure 23. Qualitative comparison between C4 and C1 with the MIMO refrigeration control system; manipulated variables.

disturbance occurred in the system. From Figure 22, system response of C4 is much faster than the first default controller C1, which benefits from the higher system bandwidth achieved by the lead-lag compensators. Furthermore, the converging speed of manipulated signals convergence is faster than the default controller C1. The quantitative indices are shown in Table 4.

DOI: 10.1021/acs.iecr.9b01854
Ind. Eng. Chem. Res. 2019, 58, 17885−17897

Table 4. Relative Indices and the Combined Indices Associated with the Qualitative Controller Comparison

index	C3 vs C1	C4 vs C1	C4 vs C2
$RIAE_1(C_{new}, C_{old})$	0.4947	0.2187	0.6230
$RIAE_2(C_{new}, C_{old})$	0.5046	0.2187	0.6238
$RITAE_1(C_{new}, C_{old}, t_{c1}, t_{s1})$	1.0031	0.0524	0.0325
$RITAE_2(C_{new}, C_{old}, t_{c2}, t_{s2})$	1.0003	0.1032	0.5640
$RIAE_2(C_{new}, C_{old}, t_{c3}, t_{s3})$	0.6904	0.2216	0.7074
$RIAE_2(C_{new}, C_{old}, t_{c4}, t_{s4})$	0.4728	0.2315	1.8077
$RIAVU_{11}(C_{new}, C_{old})$	1.2392	1.5123	1.3403
$RIAVU_{21}(C_{new}, C_{old})$	1.3303	1.5143	1.1022
$J(C_{new}, C_{old})$	0.7587	0.2876	0.6743

Controller 2 is the second competitive baseline, whose simulated results are only found in the instructive document. To exhibit the enhanced performance of our developed control strategies, the qualitative comparison results are given in Figures 24 and 25 and Table 4. Although the structure of *C*2 is

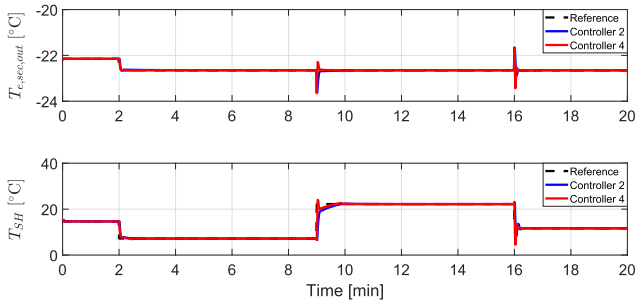

Figure 24. Qualitative comparison between *C*4 and *C*2 with the MIMO refrigeration control system; controlled variables.

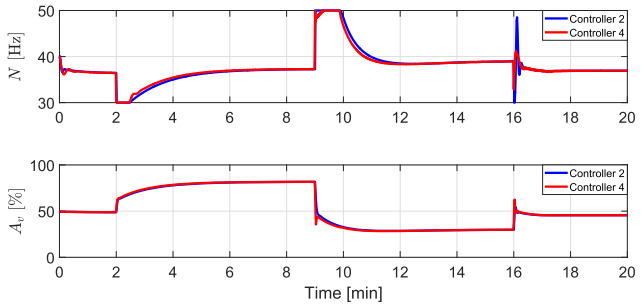

Figure 25. Qualitative comparison between *C*4 and *C*2 with the MIMO refrigeration control system; manipulated variables.

unknown, the proposed control structure still has a faster response, shorter controller saturated duration, and better index compared to *C*2.

7. CONCLUSIONS

Addressing the PID2018 Benchmark challenge, this paper focuses on the practical control design with minimal modeling efforts but enhanced system performance. The canonical one-compression-stage, one-load-demand refrigeration cycle system is first analyzed and found with low coupling degree and strong nonlinearity. To minimize the nonlinear effect with minimal modeling efforts, only nominal model is identified and two lookup tables are established to compensate the nonlinearity in terms of the steady-state gain. Based on the original control structures and parameters, the feedforward controllers are employed to compensate major disturbances $T_{e,sec,in}$ and $T_{c,sec,in}$. The detailed design procedures of the feedforward controller are also presented. Moreover, two fractional-order lead-lag compensators are then designed to increase the system bandwidth, which leads to a more aggressive system response. The parameters of the lead-lag compensators are determined by scanning the desired gain crossover frequency, phase margin of the open-loop system in a certain range. Ultimately, the simulation results and qualitative indices finally confirm the effectiveness of the fractional-order lead-lag compensators in terms of the response speed and the benefits of feedforward compensators in terms of the disturbance rejection.

AUTHOR INFORMATION

Corresponding Authors

*E-mail: jieyuan@seu.edu.cn (J.Y.).
*E-mail: ychen53@ucmerced.edu (Y.Q.C.).

ORCID

YangQuan Chen: 0000-0002-7422-5988

Notes

The authors declare no competing financial interest.

REFERENCES

(1) Jahangeer, K.; Tay, A. A.; Islam, M. R. Numerical investigation of transfer coefficients of an evaporatively-cooled condenser. *Appl. Therm. Eng.* **2011**, *31*, 1655−1663.
(2) Steemers, K.; Yun, G. Y. Household energy consumption: a study of the role of occupants. *Build. Res. Inf.* **2009**, *37*, 625−637.
(3) Yeo, Y.-K.; Kwon, T.-I. A neural PID controller for the pH neutralization process. *Ind. Eng. Chem. Res.* **1999**, *38*, 978−987.
(4) Pan, T.; Li, S.; Cai, W.-J. Lazy learning-based online identification and adaptive PID control: a case study for CSTR process. *Ind. Eng. Chem. Res.* **2007**, *46*, 472−480.
(5) Salazar, M.; Méndez, F. PID control for a single-stage transcritical CO2 refrigeration cycle. *Appl. Therm. Eng.* **2014**, *67*, 429−438.
(6) Singh, J.; Chattterjee, K.; Vishwakarma, C. Two degree of freedom internal model control-PID design for LFC of power systems via logarithmic approximations. *ISA Trans.* **2018**, *72*, 185−196.
(7) Marino, R.; Scalzi, S.; Netto, M. Nested PID steering control for lane keeping in autonomous vehicles. *Control Eng. Pract.* **2011**, *19*, 1459−1467.
(8) Ziegler, J. G.; Nichols, N. B. Optimum settings for automatic controllers. *Trans. ASME* **1942**, *64*.
(9) Monje, C. A.; Vinagre, B. M.; Feliu, V.; Chen, Y. Q. Tuning and auto-tuning of fractional order controllers for industry applications. *Control Eng. Pract.* **2008**, *16*, 798−812.
(10) Grimholt, C.; Skogestad, S. Optimal PI and PID control of first-order plus delay processes and evaluation of the original and improved SIMC rules. *J. Process Control* **2018**, *70*, 36−46.
(11) Tahoun, A. Anti-windup adaptive PID control design for a class of uncertain chaotic systems with input saturation. *ISA Trans.* **2017**, *66*, 176−184.
(12) Eltag, K.; Aslamx, M. S.; Ullah, R. Dynamic Stability Enhancement Using Fuzzy PID Control Technology for Power System. *Int. J. Control Autom. Syst.* **2019**, *17*, 234−242.
(13) Zamani, A.; Barakati, S. M.; Yousofi-Darmian, S. Design of a fractional order PID controller using GBMO algorithm for load-frequency control with governor saturation consideration. *ISA Trans.* **2016**, *64*, 56−66.
(14) Zeng, G.; Xie, X.; Chen, M.; Weng, J. Adaptive population extremal optimization-based PID neural network for multivariable nonlinear control systems. *Swarm Evolut. Comput.* **2019**, *44*, 320−334.
(15) Boubertakh, H.; Tadjine, M.; Glorennec, P. Y.; Labiod, S. Tuning fuzzy PD and PI controllers using reinforcement learning. *ISA Trans.* **2010**, *49*, 543−551.

DOI: 10.1021/acs.iecr.9b01854
Ind. Eng. Chem. Res. 2019, 58, 17885−17897

(16) Åström, K. J.; Hägglund, T. The future of PID control. *Control Eng. Pract.* **2001**, *9*, 1163−1175.
(17) Bejarano, G.; Alfaya, J. A.; Rodríguez, D.; Ortega, M. G. Benchmark for PID Control of Refrigeration Systems Based on Vapour Compression. http://www.pid18.ugent.be/, 2018.
(18) Ren, X.; Lewis, F. L.; Zhang, J.; Ge, S. S. Feedforward control based on neural networks for hard disk drives. *IEEE Trans. Magn.* **2009**, *45*, 3025−3030.
(19) Zhao, Y.; Drennen, J. K.; Mohan, S.; Wu, S.; Anderson, C. A. Feedforward and Feedback Control of a Pharmaceutical Coating Process. *AAPS PharmSciTech* **2019**, *20*, 157.
(20) Nguyen, L. M.; Chen, X. MPC Inspired Dynamical Output Feedback and Adaptive Feedforward Control Applied to Piezo-Actuated Positioning Systems. *IEEE Trans. Ind. Electron.* **2019**, 1.
(21) Liu, L.; Tian, S.; Xue, D.; Zhang, T.; Chen, Y. Industrial feedforward control technology: a review. *J. Intell. Manuf.* **2018**, *41*, No. 87.
(22) Sun, L.; Li, D.; Gao, Z.; Yang, Z.; Zhao, S. Combined feedforward and model-assisted active disturbance rejection control for non-minimum phase system. *ISA Trans.* **2016**, *64*, 24−33.
(23) Sun, L.; Shen, J.; Hua, Q.; Lee, K. Y. Data-driven oxygen excess ratio control for proton exchange membrane fuel cell. *Appl. Energy* **2018**, *231*, 866−875.
(24) Zhong, H.; Pao, L.; de Callafon, R. Feedforward control for disturbance rejection: Model matching and other methods. Proceedings of the 24th Chinese Control and Decision Conference, 2012; pp 3528−3533.
(25) Brosilow, C.; Joseph, B. *Techniques of Model-Based Control*; Prentice Hall Professional, 2002.
(26) Guzmán, J. L.; Hägglund, T.; Veronesi, M.; Visioli, A. Performance indices for feedforward control. *J. Process Control* **2015**, *26*, 26−34.
(27) Adam, E.; Marchetti, J. L. Designing and tuning robust feedforward controllers. *Comput. Chem. Eng.* **2004**, *28*, 1899−1911.
(28) Beijen, M.; Heertjes, M.; Dijk, J. V.; Hakvoort, W. Self-tuning MIMO disturbance feedforward control for active hard-mounted vibration isolators. *Control Eng. Pract.* **2018**, *72*, 90−103.
(29) Vilanova, R.; Arrieta, O.; Ponsa, P. IMC based feedforward controller framework for disturbance attenuation on uncertain systems. *ISA Trans.* **2009**, *48*, 439−448.
(30) White, M. T.; Tomizuka, M. Increased disturbance rejection in magnetic disk drives by acceleration feedforward control and parameter adaptation. *Control Eng. Pract.* **1997**, *5*, 741−751.
(31) Xie, Y.; Alleyne, A. A robust two degree-of-freedom controller for systems with both model and measurement uncertainty. *Control Eng. Pract.* **2014**, *25*, 55−65.
(32) Dorf, R. C.; Bishop, R. H. *Modern Control Systems*; Pearson, 2011.
(33) Monje, C. A.; Calderon, A. J.; Vinagre, B. M.; Feliu, V. The Fractional Order Lead Compensator. Second IEEE International Conference on Computational Cybernetics, 2004; pp 347−352.
(34) Khiabani, A. G.; Babazadeh, R. Design of robust fractional-order lead-lag controller for uncertain systems. *IET Control Theory Appl.* **2016**, *10*, 2447−2455.
(35) Yu, Z.; Wang, J. Performance assessment of static lead-lag feedforward controllers for disturbance rejection in PID control loops. *ISA Trans.* **2016**, *64*, 67−76.
(36) Yuan, J.; Ates, A.; Dehghan, S.; Zhao, Y.; Fei, S.; Chen, Y. Q. PID2018 Benchmark Challenge: Model-based Feedforward Compensator with A Conditional Integrator. *IFAC-PapersOnLine* **2018**, *51*, 888−893.
(37) MacArthur, J. W.; Meixel, G. D.; Shen, L. S. Application of numerical methods for predicting energy transport in earth contact systems. *Appl. Energy* **1983**, *13*, 121−156.
(38) McKinley, T. L.; Alleyne, A. G. An advanced nonlinear switched heat exchanger model for vapor compression cycles using the moving-boundary method. *Int. J. Refrig.* **2008**, *31*, 1253−1264.
(39) Li, B.; Alleyne, A. G. A dynamic model of a vapor compression cycle with shut-down and start-up operations. *Int. J. Refrig.* **2010**, *33*, 538−552.
(40) Pangborn, H.; Alleyne, A. G.; Wu, N. A comparison between finite volume and switched moving boundary approaches for dynamic vapor compression system modeling. *Int. J. Refrig.* **2015**, *53*, 101−114.
(41) Bristol, E. On a new measure of interaction for multivariable process control. *IEEE Trans. Autom. Control* **1966**, *11*, 133−134.
(42) Zames, G. Unstable Systems and Feedback: The Gap Metric. Proceedings of the Allerton Conference, 1980; pp 380−385.
(43) El-Sakkary, A. The gap metric: Robustness of stabilization of feedback systems. *IEEE Trans. Autom. Control* **1985**, *30*, 240−247.
(44) Du, J.; Johansen, T. A. Integrated multilinear model predictive control of nonlinear systems based on gap metric. *Ind. Eng. Chem. Res.* **2015**, *54*, 6002−6011.
(45) Galán, O.; Romagnoli, J. A.; PalazoÇğlu, A.; Arkun, Y. Gap metric concept and implications for multilinear model-based controller design. *Ind. Eng. Chem. Res.* **2003**, *42*, 2189−2197.
(46) Arslan, E.; Çamurdan, M. C.; Palazoglu, A.; Arkun, Y. Multimodel scheduling control of nonlinear systems using gap metric. *Ind. Eng. Chem. Res.* **2004**, *43*, 8275−8283.

DOI: 10.1021/acs.iecr.9b01854
Ind. Eng. Chem. Res. 2019, 58, 17885−17897